

# SECUREGS: BOOSTING THE SECURITY AND FIDELITY OF 3D GAUSSIAN SPLATTING STEGANOGRAPHY

**Anonymous authors**

Paper under double-blind review

## ABSTRACT

3D Gaussian splatting (3DGS) has emerged as a premier method for 3D representation due to its real-time rendering and high-quality outputs, underscoring the critical need to protect the copyright and privacy of 3D assets. Traditional NeRF steganography methods fail to address the explicit nature of 3DGS since its point cloud files are publicly accessible. Existing GS steganography solutions mitigate some issues but still struggle with reduced rendering fidelity, increased computational demands, and security flaws, especially in the security of the geometric structure of the visualized point cloud. To address these challenges, we propose a **SecureGS**, a secure and efficient 3DGS steganography framework inspired by Scaffold-GS’s anchor point design and neural decoding. SecureGS utilizes a hybrid decoupled Gaussian encryption mechanism to embed offsets, scales, rotations, and RGB attributes of the hidden 3D Gaussian points within anchor point features, retrievable only by authorized users through privacy-preserving neural networks. To further enhance security, we propose a density region-aware anchor growing and pruning strategy that adaptively locates optimal hiding regions without exposing hidden information. Extensive experiments demonstrate that SecureGS significantly surpasses existing GS steganography methods in rendering fidelity, speed, and security, effectively concealing and accurately extracting 3D objects, images, and bits within original 3D scenes.

## 1 INTRODUCTION

Benefiting from its real-time rendering capabilities and impressive rendering quality, 3D Gaussian splatting (3DGS) has become a mainstream 3D representation approach. Since optimizing a 3D scene requires a large amount of computing resources and 3D tampering approaches are developing rapidly, protecting the copyright and privacy of 3D assets is particularly important. As an emerging research field, 3DGS steganography aims to embed bits, images, or 3D content into 3D Gaussian points invisibly, and extract them losslessly in the decoding end. It has great potential for application in encrypted communications, copyright protection, identity verification, and forensic analysis.

As a preliminary work for 3DGS steganography, previous works on NeRF watermarking have achieved excellent results. For instance, StegaNeRF (Li et al., 2023a) jointly finetuned the weights of NeRF and a decoder so that each 2D rendered view can decode the pre-defined watermark. CopyRNeRF (Luo et al., 2023b) and WateRF (Jang et al., 2024a) focused on bit hiding and robust decryption and can achieve copyright traceability of NeRF via a 2D view. However, these methods that work on implicit representation cannot be effectively applied to 3DGS steganography, since 3DGS is an explicit representation and its point cloud files are often made public and transparent for online real-time rendering.

To achieve this demand, GS-Hider (Zhang et al., 2024b) utilized a coupled feature field and neural decoders to simultaneously render the original and hidden scene, as shown in Fig. 1(a). However, it presents several shortcomings in terms of fidelity, security, and rendering speed. **Fidelity:** Representing the original scene and hidden information using the same set of Gaussian points with a compact feature attribute will easily lead to mutual interference, especially when the geometry of the hidden information is inconsistent with that of the original scene, resulting in suboptimal rendering fidelity. **Rendering Speed:** Due to the use of convolutional networks to decode the rendered coupled feature fields, there is an increase in computational complexity, which affects the rendering speed of 3DGS

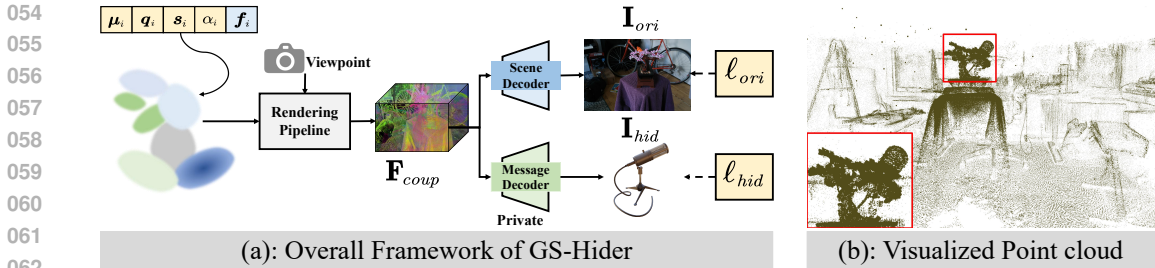


Figure 1: Analysis of previous 3DGS steganography method GS-Hider (Zhang et al., 2024b).

steganography to a certain extent. **Security:** We categorize the security of GS steganography into two types, namely file format security and geometric structure security. Format security means that the published 3DGS point cloud does not add any additional attributes that could arouse suspicion or lead to deletion by malicious abusers. Geometric structure security denotes when visualizing the Gaussian point cloud, no traces of the hidden scene’s geometric structure are revealed. The latter is what GS-Hider cannot achieve, which may pose a risk of leaking hidden messages (such as Fig. 1(b)).

Our insight for solving these problems comes from a successful variant of 3DGS, namely Scaffold-GS (Lu et al., 2023). Scaffold-GS uses anchor points to establish a hierarchical and region-aware 3D scene representation. Then, a set of neural Gaussians with learnable attributes are dynamically predicted from the anchor feature via several simple MLPs. Scaffold-GS is naturally suited for steganography for two reasons: **First**, it uses implicit MLPs to store Gaussian point attributes, allowing encryption to focus on MLPs rather than explicit Gaussian points, making it ideal for steganography. **Second**, it maintains comparable rendering quality and real-time performance to 3DGS, preserving its high fidelity and fast rendering benefits.

To address the limitations of existing 3DGS steganography methods, we propose a more secure and efficient 3DGS steganography framework, dubbed **SecureGS**. Fig. 2 presents our overall pipeline and application scenario. Specifically, we design a hybrid decoupled Gaussian encryption representation capable of decoding two sets of dense Gaussian points from a sparse set of anchor points, which are used for rendering the original scene and the hidden object, respectively. Note that we specifically introduce a privacy-preserving offset predictor to conceal the positions of the hidden Gaussian points. Furthermore, to prevent the geometric structure of the hidden object from being exposed in the anchor point cloud, we innovatively propose a density region-aware anchor growing strategy. Based on the gradient of the joint rendering loss, it can adaptively find the location of hidden 3D objects, thereby lowering the splitting threshold in that region and allowing the original scene’s anchors to cover the hidden anchor points safely. In a nutshell, our contributions are summarized as follows.

- (1) We present a novel attempt to introduce neural voxelization into the 3DGS steganography, realizing a more secure, high-fidelity, and efficient framework **SecureGS**. It can effectively hide 3D objects, images, and bits within the original 3D scene and precisely extract them.
- (2) We develop a hybrid decoupled Gaussian encryption representation that can hide and predict the location and attributes of the hidden Gaussian points via a set of neural decoders, ensuring that the overall framework maintains a format consistency in the point cloud files and is efficient in rendering hidden message and preserving the original scene.
- (3) We propose a region-aware density optimization that can locate hidden 3D positions and promote anchor growth in that region while inhibiting pruning, thereby significantly enhancing the geometric structure security of the point cloud within the overall framework.
- (4) Extensive experiments demonstrate that our method significantly outperforms existing 3D steganography methods in terms of the fidelity of container 3DGS, rendering speed, and security.

## 2 RELATED WORKS

### 2.1 3D GAUSSIAN SPLATTING

3D Gaussian Splatting (3DGS) (Kerbl et al., 2023) has emerged as a highly effective approach for 3D scene reconstruction, utilizing millions of 3D Gaussians. Starting from a set of Structure-from-Motion

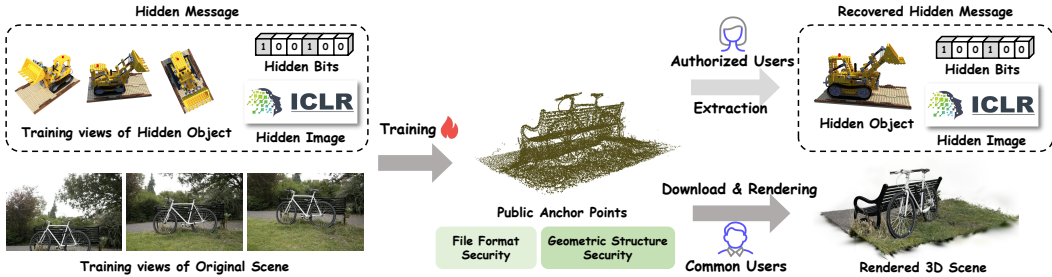


Figure 2: Overall Pipeline of our SecureGS. 3D objects, images, and bits can be hidden in the original 3D scene, and only authorized users can decode these hidden messages. The core of our method is to ensure both the file format and geometric structure security of the public anchor points.

(SfM) points, each point is assigned as the center (mean)  $\mu$  of a 3D Gaussian distribution:

$$\mathcal{G}(\mathbf{x}) = e^{-\frac{1}{2}(\mathbf{x}-\mu)^\top \Sigma^{-1}(\mathbf{x}-\mu)}, \quad \Sigma = \mathbf{R}\mathbf{S}\mathbf{S}^\top \mathbf{R}^\top, \quad (1)$$

where  $\mathbf{x}$  is a position within the 3D scene and  $\Sigma$  denotes the covariance matrix of the 3D Gaussian, which is formulated using a scaling matrix  $\mathbf{S}$  and rotation matrix  $\mathbf{R}$ . Instead of using the resource-intensive ray-marching, 3DGS efficiently renders the scene via a tile-based rasterizer. Specifically, the 3D Gaussian  $\mathcal{G}(\mathbf{x})$  are first transformed to 2D Gaussians  $\mathcal{G}'(\mathbf{x})$  on the image plane via the projection mechanism (Zwicker et al., 2001). Let  $\mathbf{C} \in \mathbb{R}^{H \times W \times 3}$  represent the color of the rendered image where  $H$  and  $W$  represent the height and width of images, the  $\alpha$ -blending process of a tile-based rasterizer is outlined as follows:

$$\mathbf{C}[\mathbf{p}] = \sum_{i=1}^N c_i \sigma_i \prod_{j=1}^{i-1} (1 - \sigma_j), \quad \sigma_i = \alpha_i \mathcal{G}'_i(\mathbf{p}), \quad (2)$$

where  $\mathbf{p} = (u, v)$  is the queried pixel position and  $N$  denotes the number of sorted 2D Gaussians associated with the queried pixel.  $c_i$  and  $\alpha_i$  respectively denote the color and opacity component of the Gaussian point. In contrast to previous implicit representations, 3DGS dramatically improves both training speed and rendering efficiency. To further elevate 3DGS’s rendering capabilities, Mip-Splatting (Yu et al., 2023b) introduced 2D and 3D filtering, enabling high-quality, alias-free rendering across arbitrary resolutions. Moreover, Scaffold-GS (Lu et al., 2023) integrated structured neural anchors to enhance the rendering quality from diverse perspectives. The exceptional performance of 3DGS has extended its utility to a broad range of applications, including SLAM (Keetha et al., 2023; Matsuki et al., 2023), 4D reconstruction (Li et al., 2023b; Luiten et al., 2023; Wu et al., 2023; Yang et al., 2024b), and 3D content generation (Tang et al., 2023; Yi et al., 2024; Yang et al., 2024a).

## 2.2 3D STEGANOGRAPHY

Steganography has undergone significant evolution over the decades (Provos & Honeyman, 2003; Cheddad et al., 2010). With the rise of deep learning, numerous deep steganography methods have been developed to invisibly embed messages into various carriers and reliably extract them, spanning 2D images (Zhang et al., 2024a; Zhu et al., 2018; Baluja, 2019; Yu et al., 2023a), videos (Zhang et al., 2024c; Luo et al., 2023a), audio (Liu et al., 2023a;b; Chen et al., 2023; Roman et al., 2024), and even generative models (Wen et al., 2024; Fernandez et al., 2023). Traditional 3D steganography has primarily focused on watermarking explicit 3D representations, such as meshes (Ohbuchi et al., 2002; Praun et al., 1999; Wu et al., 2015), typically by perturbing vertices or transforming data into the frequency domain. Additionally, Yoo et al. (Yoo et al., 2022) proposed a method to extract copyright information from individual 2D perspectives, even without the full 3D mesh.

Recently, NeRF watermarking has garnered increased attention (Luo et al., 2023b; Jang et al., 2024a; Li et al., 2023a). For instance, StegaNeRF (Li et al., 2023a) embedded images or audio within 3D scenes by fine-tuning NeRF’s weights, while CopyRNeRF (Luo et al., 2023b) introduced a watermarked color representation and a distortion-resistant rendering strategy to ensure robust message extraction. WaterRF (Jang et al., 2024a) leveraged deferred backpropagation with patch loss and employed discrete wavelet transform to enhance fidelity and robustness. NeRFProtector (Song et al., 2024) utilized a watermarking base model and progressive global distillation to explore relations

162 between rendering strategies and watermark embedding. Targeted at 3DGS, GS-Hider (Zhang et al.,  
 163 2024b) used coupled feature fields and neural decoders to render the original and hidden scene,  
 164 achieving high-quality 3D scene hiding. Meanwhile, GaussianStego (Li et al., 2024) proposed a  
 165 generalized pipeline for information hiding and recovery in the 3D generation model. 3D-GSW (Jang  
 166 et al., 2024b) presented a frequency-guided Densification strategy for robust watermarking in 3DGS.  
 167 However, these methods do not take into account the security of point clouds, and the fidelity of  
 168 container 3DGS is unsatisfactory.

### 170 3 METHODOLOGY

#### 172 3.1 ANALYSIS OF THE PREVIOUS 3DGS STEGANOGRAPHY METHOD

174 We first review the recent 3DGS steganography work GS-Hider. As shown in Fig. 1(a), GS-Hider  
 175 follows a “coupling-decoupling” process. It replaces the spherical harmonic coefficients in 3DGS  
 176 with a coupled feature attribute  $\mathbf{f}_i \in \mathbb{R}^{16}$  and utilizes a high-dimensional rendering pipeline to  
 177 render it as a coupled feature field  $\mathbf{F}_{coup} \in \mathbb{R}^{H \times W \times 16}$ . Furthermore, we use a public scene decoder  
 178 and a private message decoder to decouple  $\mathbf{I}_{ori} \in \mathbb{R}^{H \times W \times 3}$  and  $\mathbf{I}_{hid} \in \mathbb{R}^{H \times W \times 3}$  from  $\mathbf{F}_{coup}$ ,  
 179 respectively. Finally, we use the combination of  $\ell_{ori}$  and  $\ell_{hid}$  to constrain the optimization of the  
 180 learnable attributes of Gaussian points and the weights of two decoders.

181 Although GS-Hider achieves good rendering quality and the public point cloud file does not exhibit  
 182 suspicious attributes in terms of format, when we visualize GS-Hider’s point cloud, the geometric  
 183 structure of the hidden information is exposed in the public point cloud. For example, as shown  
 184 in Fig. 1(b), we observe that when attempting to hide the “mic” in the “bonsai”, the shape of the  
 185 microphone appears in the public point cloud file. This is because GS-Hider uses the same set of  
 186 points to represent both the original scene and the hidden object, inevitably resulting in geometric and  
 187 spatial position overlap. Moreover, GS-Hider does not implement an appropriate optimization strategy  
 188 to control the growth of Gaussian points used to render the hidden message, which exacerbates the  
 189 compromise of point cloud security.

#### 192 3.2 TASK SETTINGS AND OUR OBJECTIVES

192 Following the setup of GS-Hider (Zhang et al., 2024b), we aim for the SecureGS framework to  
 193 maintain transparency and generalization. **Transparency** denotes that after users embed information  
 194 into the original 3D scene, they can openly publish the container 3DGS for online rendering, while  
 195 preventing unauthorized users from decrypting the hidden information. **Generalization** refers to the  
 196 framework’s ability to adapt to hiding information in 3D objects, images, and bits. To be noted, unlike  
 197 GS-Hider, we aim to ensure both the **file format security** and the **geometric structure security** of  
 198 the container 3DGS point cloud file. Considering that hiding a large-scale 3D scene makes it difficult  
 199 to ensure that the point cloud structure remains confidential, we only hide a 3D object within the 3D  
 200 scene. **Fig. 2 presents our task settings and realized functions.**

#### 202 3.3 HYBRID DECOUPLED GAUSSIAN ENCRYPTION REPRESENTATION

203 Similar to previous approaches (Lu et al., 2023), we use the sparse point cloud produced by COLMAP  
 204 as the initial input and voxelize the scene, forming the voxel centers  $\mathbf{V} \in \mathbb{R}^{N \times 3}$ . Each voxel  
 205 center  $v \in \mathbf{V}$  is treated as an anchor point and equipped with a local context feature  $\mathbf{f}_v \in \mathbb{R}^{32}$ ,  
 206 a scaling factor  $\mathbf{l}_v \in \mathbb{R}^3$ , and two groups of learnable offsets  $\{\mathbf{O}_{v \otimes i}^{ori}\}_{i=1}^k$  and  $\{\mathbf{O}_{v \otimes j}^{hid}\}_{j=1}^k$ , which  
 207 respectively generates the dense Gaussian points representing the original scene and hidden object.  
 208 To avoid the format inconsistency between the container point cloud file and the original Scaffold-GS  
 209 caused by explicitly storing  $\{\mathbf{O}_{v \otimes j}^{hid}\}_{j=1}^k$ , we design an explicit-implicit hybrid Gaussian encryption  
 210 representation, as shown in Fig. 3. For the Gaussian points representing the original scene, we  
 211 explicitly store  $k$  learnable offsets  $\{\mathbf{O}_{v \otimes i}^{ori}\}_{i=1}^k$  for each anchor point  $\mathbf{x}_v$ , and use a scaling factor  $\mathbf{l}_v$   
 212 to determine the position of each Gaussian point  $\{\boldsymbol{\mu}_{v \otimes i}^{ori}\}_{i=1}^k$ .

$$213 \{\boldsymbol{\mu}_{v \otimes 0}^{ori}, \dots, \boldsymbol{\mu}_{v \otimes (k-1)}^{ori}\} = \mathbf{x}_v + \{\mathbf{O}_{v \otimes 0}^{ori}, \dots, \mathbf{O}_{v \otimes (k-1)}^{ori}\} \cdot \mathbf{l}_v, \quad (3)$$

214 Additionally, we adopt an implicit neural decoder  $\mathcal{F}_o^\dagger$  to store the offsets of Gaussian points that  
 215 render the hidden object. Following (Lu et al., 2023), we also extend  $\mathbf{f}_v$  to be multi-resolution and

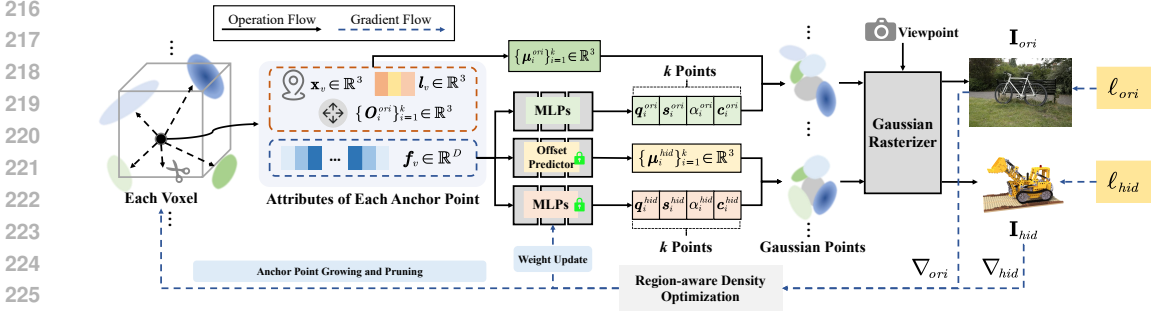


Figure 3: Overall framework of our SecureGS. We first voxelize the scene, where each voxel contains an anchor point with the position  $\mathbf{x}_v$ , feature  $\mathbf{f}_v$ , scaling factor  $l_v$ , and offsets  $\{O_{v\otimes i}^{ori}\}_{i=1}^k$ . Then, we explicitly compute the positions  $\mu_{v\otimes i}^{ori}$  via Eq. 3, and predict attributes  $\{c_{v\otimes i}^{ori}, \alpha_{v\otimes i}^{ori}, \mathbf{q}_{v\otimes i}^{ori}, \mathbf{s}_{v\otimes i}^{ori}\}$  via a series of public MLPs. Meanwhile, we use private offset predictor  $\mathcal{F}_o^\dagger$  and MLPs to store the position and attributes of the Gaussian points representing the hidden object. Finally, we design a region-aware density optimization to control the Gaussian point growing and pruning.

view-dependent blended feature  $\hat{\mathbf{f}}_v$ . Given the camera located at  $\mathbf{x}_c$  and an anchor at  $\mathbf{x}_v$ , the hidden offsets are computed as follows:

$$\{\mu_{v\otimes 0}^{hid}, \dots, \mu_{v\otimes (k-1)}^{hid}\} = \mathbf{x}_v + \mathcal{F}_o^\dagger(\hat{\mathbf{f}}_v, \delta_{vc}, \vec{d}_{vc}), \quad (4)$$

where  $\delta_{vc} = \|\mathbf{x}_v - \mathbf{x}_c\|_2$  denotes the relative distance and  $\vec{d}_{vc} = (\mathbf{x}_v - \mathbf{x}_c) / \|\mathbf{x}_v - \mathbf{x}_c\|_2$  denotes the viewing direction. The offset predictor  $\mathcal{F}_o^\dagger$  will only be accessible to authorized users.

Furthermore, we use a set of public MLPs  $\{\mathcal{F}_c, \mathcal{F}_\alpha, \mathcal{F}_q, \mathcal{F}_s\}$  to predict the opacity  $\alpha_{v\otimes i}^{ori} \in \mathbb{R}^1$ , quaternion  $\mathbf{q}_{v\otimes i}^{ori} \in \mathbb{R}^4$ , scaling  $\mathbf{s}_{v\otimes i}^{ori} \in \mathbb{R}^3$  and color  $\mathbf{c}_{v\otimes i}^{ori} \in \mathbb{R}^3$  of the Gaussian points representing the original scene and adopt the private MLPs  $\{\mathcal{F}_c^\dagger, \mathcal{F}_\alpha^\dagger, \mathcal{F}_q^\dagger, \mathcal{F}_s^\dagger\}$  to produce  $\{\alpha_{v\otimes j}^{hid}, \mathbf{q}_{v\otimes j}^{hid}, \mathbf{s}_{v\otimes j}^{hid}, \mathbf{c}_{v\otimes j}^{hid}\}$  that render the hidden object. We take the color component as an example.

$$\{c_{v\otimes 0}^{ori}, \dots, c_{v\otimes (k-1)}^{ori}\} = \mathcal{F}_c(\hat{\mathbf{f}}_v, \delta_{vc}, \vec{d}_{vc}), \{c_{v\otimes 0}^{hid}, \dots, c_{v\otimes (k-1)}^{hid}\} = \mathcal{F}_c^\dagger(\hat{\mathbf{f}}_v, \delta_{vc}, \vec{d}_{vc}). \quad (5)$$

Similarly, other attributes of SecureGS can also be produced by these MLPs based on the blended features, the distance, and the viewing direction. Finally, all 3D Gaussian points are rendered into 2D views of the original scene  $\mathbf{I}_{ori}$  and the hidden object  $\mathbf{I}_{hid}$  via the rasterizer and alpha blending mechanism similar to 3DGS (Kerbl et al., 2023).

### 3.4 REGION-AWARE DENSITY OPTIMIZATION

**Motivation:** Although our hybrid Gaussian encryption mechanism can securely represent the hidden Gaussian points in format, we find that by visualizing the anchor point cloud, the clues of the hidden object can still be discovered from the geometric structure, as shown in Fig. 4. For instance, since the anchor point cloud is relatively sparse, when we hide the 3D object “hot dog” in the “bicycle” scene, the geometric structure of the hot dog is completely exposed, which seriously poses a significant security risk. To address this issue, a straightforward solution is to increase the density of Gaussian points, allowing the Gaussian points of the original scene to obscure those of the hidden object. However, this indiscriminate approach of promoting Gaussian point splitting significantly increases the number of anchor points, leading to slower rendering speeds and higher storage costs.

To overcome the trade-off between the storage size and geometry structure security of the container point cloud, we propose a region-aware density optimization strategy to control the splitting and pruning of the Gaussian points adaptively. It can change the threshold of anchor point splitting so that



Figure 4: Visualization of the point cloud produced by our SecureGS without region-aware density optimization (RDO) strategy. The RGB reference of the hidden scene is placed on the left bottom.

Gaussian anchor points only grow in large quantities at the location of hidden objects while having a small impact on the rendering and storage efficiency of the overall framework. Specifically, our anchor growing strategy can be divided into three steps: **1) Asynchronous Gradient calculation:** As shown in Fig. 3, for the optimization of both the original scene and the hidden 3D object, we separately accumulate the gradients of the neural Gaussian points involved in backward with different frequencies, denoted as  $\nabla_{ori}$  and  $\nabla_{hid}$ . We aim to slow down the accumulation of  $\nabla_{hid}$ , thereby suppressing the splitting of the hidden anchor points and enhancing security. **2) Obtain a high-density region:** Since we calculate  $\nabla_{ori}$  and  $\nabla_{hid}$  separately, we can also perform anchor growing based on  $\nabla_{ori}$  and  $\nabla_{hid}$  in a decoupled manner. For example, if  $\nabla_{hid} > \tau_{fix}$ , we will split new anchor points, forming the point set  $\Gamma_{hid}$ . Note that  $\tau_{fix}$  denotes a pre-set splitting threshold. Similarly, we can construct  $\Gamma_{ori}$  using  $\nabla_{ori} > \tau_{fix}$  as the trigger condition. Afterward, we apply a point cloud clustering algorithm DBSCAN (Ester et al., 1996) on these hidden anchor points  $\Gamma_{hid}$  to obtain a bounding box  $\mathbb{S}_{bbx}$  where the hidden anchor points are densely distributed. **3) Growing and pruning for  $\Gamma_{ori}$  and  $\Gamma_{hid}$ :** For the growing of  $\Gamma_{ori}$ , we replace the fixed threshold  $\tau_{fix}$  with an adaptive threshold  $\tau_{ada}$  for splitting based on whether the points are within the bounding box  $\mathbb{S}_{bbx}$ .

$$\tau_{ada} = \tau_{fix} / r_{down}, \text{ if } (x, y, z) \in \mathbb{S}_{bbx} \text{ or } \tau_{fix} \text{ else,} \quad (6)$$

where  $(x, y, z)$  denotes the spatial coordinates of an anchor point.  $r_{down}$  denotes a gradient down-sampling ratio. Then, we prune some of the anchor points in  $\Gamma_{ori} \cup \Gamma_{hid}$  if an anchor fails to produce neural Gaussians with a satisfactory level of opacity. Note that we still use  $\tau_{fix}$  as the threshold for the growing of  $\Gamma_{hid}$  in this stage. The complete algorithm is presented in Alg. 1.

### 3.5 TRAINING DETAILS AND LOSS FUNCTIONS

To train the proposed SecureGS, we use the pixel-level  $\ell_1$  loss, SSIM term  $\ell_{ssim}$  and volume regularization  $\ell_{vol}$  (Lu et al., 2023) to optimize the learnable attributes of anchor points and the weights of MLPs  $\{\mathcal{F}_c, \mathcal{F}_\alpha, \mathcal{F}_q, \mathcal{F}_s, \mathcal{F}_o^\dagger, \mathcal{F}_c^\dagger, \mathcal{F}_\alpha^\dagger, \mathcal{F}_q^\dagger, \mathcal{F}_s^\dagger\}$ . Given the ground truth of the original training view  $\hat{\mathbf{I}}_{ori}$  and its corresponding hidden view  $\hat{\mathbf{I}}_{hid}$ , the supervision is expressed as follows.

$$\ell_{ori} = (1 - \alpha) \cdot \ell_1(\mathbf{I}_{ori}, \hat{\mathbf{I}}_{ori}) + \alpha \cdot \ell_{ssim}(\mathbf{I}_{ori}, \hat{\mathbf{I}}_{ori}) + \beta \cdot \ell_{vol}(\mathbf{s}^{ori}), \quad (7)$$

$$\ell_{hid} = (1 - \alpha) \cdot \ell_1(\mathbf{I}_{hid}, \hat{\mathbf{I}}_{hid}) + \alpha \cdot \ell_{ssim}(\mathbf{I}_{hid}, \hat{\mathbf{I}}_{hid}) + \beta \cdot \ell_{vol}(\mathbf{s}^{hid}), \quad (8)$$

where  $\alpha$  and  $\beta$  are used to balance the components of each loss. The volume regularization  $\ell_{vol}$  prompts the neural Gaussians to be compact with minimal overlapping via constraining the product of the scale in each Gaussian. Finally, our total loss is  $\ell_{total} = \ell_{ori} + \lambda \cdot \ell_{hid}$ , where  $\lambda$  denotes the trade-off factor to balance the rendering of the original scene and hidden object.

## 4 EXPERIMENTS

### 4.1 EXPERIMENTAL SETUP

**Dataset Preparation:** We respectively conducted experiments on hiding 3D objects, 2D images, and bits in 3D scenes or objects. For 3D object and 2D image hiding, the original scene includes the bicycle (BI.), flowers (FL.), garden (GA.), stump (ST.), treehill (TR.), room (RO.), counter (CO.), kitchen (KI.), bonsai (BO.) from Mip-NeRF 360 (Barron et al., 2021). The hidden 3D object is obtained from the Blender dataset (Mildenhall et al., 2020). We use Supersplat<sup>1</sup> to embed hidden 3D objects into 3D scenes. For bit hiding, we hide 48 bits into the 3D objects (Mildenhall et al., 2020), which is the maximum number of bits that other comparison methods can support.

**Comparison Methods:** For 3D object and 2D image hiding, we compare our SecureGS with existing 3DGS steganography method GS-Hider (Zhang et al., 2024b). Meanwhile, similar to StegaNeRF (Li et al., 2023a), we feed the output of the original 3DGS to a U-shaped decoder and constrain it to output hidden objects, thus implementing a variant called 3DGS+StegaNeRF. For bit hiding, since there is still no 3DGS steganography work for bit hiding available, we compare our method with two SOTA NeRF watermarking methods (Luo et al., 2023b; Song et al., 2024).

**Evaluation Metrics:** We utilize PSNR, SSIM, LPIPS of the original scene, and hidden message to measure the rendering quality of different methods. Meanwhile, FPS and storage size (MB) are

<sup>1</sup><https://playcanvas.com/supersplat>

Table 1: Comparison of the PSNR(dB), storage size, and FPS performance of the original scenes and hidden message. ‘‘Scene-Level’’ denotes hiding a complete RGB image where the objects are embedded in the original scene, and ‘‘Object-level’’ means hiding isolated objects without a background. The best results are highlighted in pink and the second-best ones are in yellow .

Method	Type	Size (MB)	FPS	BI.	FL.	GA.	ST.	TR.	RO.	CO.	KI.	BO.	Avg
Scaffold-GS	Ori.	161.46	142.91	25.01	21.26	27.19	26.49	22.96	32.26	29.48	31.35	32.61	27.62
3DGS +StegaNeRF	Ori.	1106.67	35.09	24.05	21.92	27.28	26.00	22.56	28.95	27.46	29.39	31.13	26.53
	Hid.			29.03	29.28	32.38	27.60	28.32	31.35	27.06	32.21	31.20	29.82
GS-Hider	Ori.	468.63	48.28	24.42	20.85	27.28	25.98	22.01	30.20	27.88	29.90	30.84	26.59
	Hid.			30.82	28.35	32.96	28.13	27.97	34.20	27.87	32.95	32.33	30.62
SecureGS (Scene-Level)	Ori.	267.39	131.71	25.33	21.34	27.28	26.73	22.93	32.36	29.94	31.51	32.33	27.75
	Hid.			33.74	30.45	34.47	30.24	29.38	35.93	30.11	33.21	32.99	32.28
SecureGS (Object-Level)	Ori.	290.54	106.98	25.31	21.37	27.51	26.75	22.91	32.51	30.28	31.70	33.05	27.93
	Hid.			48.04	40.70	38.23	29.77	50.96	38.45	30.77	33.22	33.75	38.21



Figure 5: Rendering quality comparison of the hidden message between the proposed SecureGS, previous GS-Hider, and 3DGS+StegaNeRF. For our SecureGS, we also present the decoupled original scene and hidden object on the 4<sup>th</sup> and 5<sup>th</sup> row, which cannot be achieved by other methods.

used to evaluate rendering speed and memory efficiency. Bit accuracy (%) is adopted to verify the decoding precision of our framework.

**Implementation Details:**  $\lambda$  is set to 10 when hiding 3D objects and set to 0.1 when hiding a single image.  $\alpha$  and  $\beta$  in Eq. 8 are respectively set to 0.2 and 0.01.  $\tau_{fix}$  and  $r_{down}$  are respectively set to 0.0002 and 4. We consistently set  $k = 10$  across all experiments and the MLPs used in our approach consist of 2 layers with ReLU activations with each hidden layer having 32 units. We conduct all our experiments on the NVIDIA RTX 4090Ti server and use the same rasterizer as the original 3DGS.

#### 4.2 COMPARISON WITH EXISTING 3DGS STEGANOGRAPHY METHODS

To verify the superiority of our method, we compare the proposed SecureGS with two state-of-the-art 3DGS steganography methods in hiding 3D objects in 3D scenes. Our SecureGS has significant advantages in at least the following three aspects.

**Higher rendering fidelity:** As reported in Tab. 5, our method improves the rendering quality of the original scene by 1.16dB and the fidelity of the hidden object by 1.66dB compared to GS-Hider. Furthermore, due to the utilization of more Gaussian points, the PSNR of our rendered original scene can even slightly surpass that of our baseline Scaffold-GS, which proves that our decoupled Gaussian encryption representation ensures the rendering of the hidden object and the original scene do not

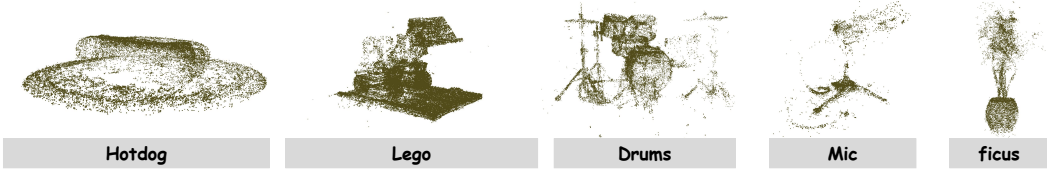


Figure 6: Visualization of the anchor point cloud of our SecureGS produced based on  $\nabla_{hid}$ .

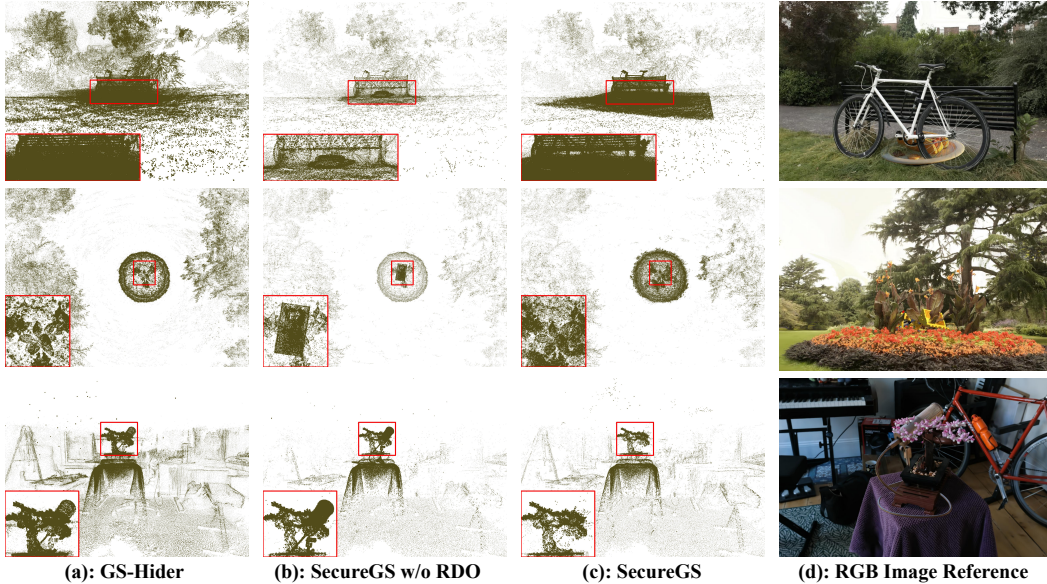


Figure 7: Visualization of the point cloud generated by GS-Hider, SecureGS without RDO strategy, and the proposed SecureGS. Clues of hidden objects cannot be found in our anchor point cloud, while the security of other methods is poor.

interfere with each other. To be noted, since GS-Hider and 3DGS+StegaNeRF decode the hidden message from a feature map or RGB image, they often suffer loss collapse when directly decoding objects with black/white backgrounds. To ensure a fair comparison with previous methods, we retained the content of the original scene when hiding objects, thus forming a complete RGB image as the  $\hat{I}_{hid}$ , and we refer to this type of hiding as “scene-level”. Meanwhile, “object-level” means that we use isolated 3D objects, without any background, as hidden content  $\hat{I}_{hid}$  for the training of our SecureGS. As shown in Fig. 5, our SecureGS demonstrates a clear advantage in scene-level hiding compared to previous methods, rendering the texture structure of hidden objects more clearly and realistically, better integrating them with the surrounding background, and producing fewer artifacts and noise. These results prove that our method achieves higher rendering quality in both subjective effects and qualitative metrics.

**Lower storage size and faster rendering speed:** As shown in Tab. 1, our SecureGS reduces storage space by 201.24MB compared to GS-Hider, and its rendering speed is nearly 3 times faster, verifying that our rendering mechanism is significantly more efficient. Compared to the original Scaffold-GS, the FPS of our SecureGS decreases by only 7% at the scene level and 25% at the object level, which is acceptable and still maintains good real-time capability.

**Decoupled original scene and hidden message decoding:** In addition to the above two performance advantages, our SecureGS can decouple the original and hidden RGB views and separate the anchor point clouds produced based on  $\nabla_{ori}$  and  $\nabla_{hid}$ . As shown in Fig. 6, the hidden anchor point decoded by our method retains a good geometry structure and is very close to the input hidden object, which greatly increases the flexibility and practicality of our framework.

### 4.3 SECURITY ANALYSIS

We analyze the security of SecureGS from three aspects. From the view of the point cloud file format, our SecureGS only stores the feature of anchor points  $f_v$ , along with the offset  $\{O_{v\otimes i}^{ori}\}_{i=1}^k$  and



Table 2: Robustness analysis under different pruning ratios.  $\text{PSNR}_o$  and  $\text{PSNR}_h$  denote the fidelity of original and hidden message.

Pruning Ratio	$\text{PSNR}_o$	$\text{SSIM}_o$	$\text{PSNR}_h$	$\text{SSIM}_h$
5%	27.41	0.814	37.45	0.985
15%	26.30	0.794	35.43	0.983
20%	24.96	0.765	33.90	0.981

Table 3: Rendering quality and bit accuracy comparison between our SecureGS and other competitive methods on Blender dataset.

Methods	Bit Acc. $\uparrow$	PSNR $\uparrow$	SSIM $\uparrow$	LPIPS $\downarrow$
CopyRNeRF	62.15	25.50	0.907	0.089
NeRFProtector	92.69	29.26	0.939	0.048
SecureGS	100.00	33.84	0.968	0.003

scaling factor  $l_v$  of the Gaussian points used for rendering the original scene, which is identical to the file format of the original Scaffold-GS. From the view of the visualized point cloud structure, as shown in Fig. 7, almost no traces of the hidden scene can be detected in our anchor points, whereas other methods fail to achieve this. For instance, when we hide a microphone in the ‘‘bonsai’’ scene (the third line in Fig. 7), GS-Hider, lacking explicit control of point cloud growing, reveals the shape of the microphone in the visualized point cloud. Similarly, if SecureGS does not employ our region-aware density optimization (RDO), the hidden message would also be exposed due to the use of sparse anchor point clouds. From the view of rendered images, as shown in Fig. 5, the rendered scene does not reveal any artifacts or edges of the hidden object and maintains a high fidelity. Therefore, we can conclude that our SecureGS is secure and reliable.

#### 4.4 ROBUSTNESS ANALYSIS

To evaluate the robustness of our SecureGS, We perform random pruning on the anchor Gaussian points. To be noted, random pruning denotes randomly pruning a proportion of anchor points. PSNR and SSIM results of the original scene ( $\text{PSNR}_o$ ,  $\text{SSIM}_o$ ) and hidden object ( $\text{PSNR}_h$ ,  $\text{SSIM}_h$ ) are reported in Tab. 2. We can find that randomly pruning 5% of anchors has almost no effect on the rendering quality of SecureGS. Even at a larger pruning rate of 25%, our method can still achieve 24.96 dB / 33.90 dB on  $\text{PSNR}_o$  /  $\text{PSNR}_h$ , which verifies that our method is robust enough to the degradation of point clouds. **More visualized results are presented in the appendix.**

#### 4.5 ABLATION STUDIES

We conduct ablation studies on two key modules of our SecureGS: hybrid decoupled Gaussian encryption representation (HDGER) and region-aware density optimization (RDO). Since both HDGER and RDO are essential components for ensuring the security of SecureGS, we only focus on exploring how adding these two modules affects the rendering fidelity of the hidden message and the original scene. By removing HDGER, we directly use an explicit  $\mathcal{O}_{v \otimes j}^{hid}$  to store the offsets of the hidden Gaussian points, referred to as ‘‘Ours w/o HDGER’’. As reported in Tab. 4, ‘‘Ours w/o HDGER’’ has almost no significant impact on the rendering quality of SecureGS. Meanwhile, when RDO is removed, we observe a 2.21dB gain on PSNR of the hidden scene due to the lack of restrictions on the splitting of hidden Gaussian points. However, the rendering quality of the original SecureGS remains satisfactory when weighed against the security enhancements provided by RDO. **Removing both modules, although the fidelity of the hidden object further improves, the security of our method is significantly compromised (as shown in Fig. 9 of the appendix).**

Table 4: Ablation studies on two key modules of our SecureGS, namely HDGER and RDO.

Method	Size(MB)	$\text{PSNR}_o$	$\text{SSIM}_o$	$\text{PSNR}_h$	$\text{SSIM}_h$
Ours w/o HDGER and RDO	185.79	27.85	0.817	40.51	0.992
Ours w/o HDGER	254.91	27.81	0.814	38.68	0.988
Ours w/o RDO	168.75	27.49	0.805	40.42	0.991
Ours	290.54	27.93	0.822	38.21	0.986

#### 4.6 EXTENSIONS

In addition to hiding 3D objects in 3D scenes, our SecureGS is also applicable to hiding bits, and single images in the original scene.

**Hiding bits in 3D Scene:** To achieve efficient hiding and lossless decoding of bit information, we introduce an additional, private MLP  $\mathcal{F}_b^\dagger$  based on the original Scaffold-GS.  $\mathcal{F}_b^\dagger$  takes the feature  $f_v \in \mathbb{R}^{32}$  of each voxel as input to convert the high-dimensional features into a specific bit length. Finally, we use the average of the bit sequences decoded from all voxels as the final copyright. The bit accuracy and rendering quality of our method and other competitive methods are presented in

Table 5: Rendering quality comparison (PSNR (dB)) of the original scene and hidden image.

Method	Type	Size (MB)	FPS	BI.	FL.	GA.	ST.	TR.	RO.	CO.	KI.	BO.	Avg
3DGS +StegaNeRF	Ori.	842.51	52.94	18.44	15.95	21.93	20.86	18.25	23.94	23.21	21.58	24.52	20.96
	Hid.			37.95	35.82	37.23	36.21	38.85	40.92	38.79	39.51	40.16	38.38
GS-Hider	Ori.	385.41	57.35	24.38	20.74	26.84	25.91	21.92	30.49	28.75	29.72	31.05	26.64
	Hid.			40.25	45.19	40.28	41.54	40.19	40.56	42.72	42.06	46.66	42.16
SecureGS	Ori.	155.09	144.46	24.86	21.02	27.07	26.21	22.86	31.96	29.13	30.52	31.70	27.26
	Hid.			45.40	47.11	38.87	42.99	39.70	41.27	42.95	41.92	46.76	42.99



Figure 8: Visualization of the rendered scene and recovered image produced by our SecureGS and other methods. Hidden view denotes the specific view that is used to hide the image.

Tab. 3. Compared to CopyRNeRF (Luo et al., 2023b) and NeRFProtector (Song et al., 2024), we can achieve 100% bit decoding accuracy because we can decode directly from the point cloud and the bits decoded from each voxel can be cross-validated. However, other methods decode bits from the 2D view with certain errors. Meanwhile, after adding bits, the fidelity of our method can still reach 33.84 dB on PSNR, which far exceeds CopyRNeRF and NeRFProtector. **Note that both these methods use a message decoder for image watermarking, they possess unique advantages in the generalization of message extraction.**

**Hiding a single image in 3D Scene:** Hiding a single image is a special case of hiding 3D objects. Here, our task is to embed a copyrighted image in a specific view of a 3D scene. Similar to GS-Hider (Zhang et al., 2024b), during the fitting of the original scene, we only encourage the rendering result at this specific view to be close to the hidden image in each iteration, without constraining other views. The results are reported in Tab. 5. It can be seen that our method outperforms GS-Hider by 0.62dB and 0.83dB on the PSNR of the original scene and restored image with a smaller storage space and a faster rendering speed. As plotted in Fig. 8, our rendered original view can achieve more detailed reconstruction, especially in some areas with complex textures such as grass, while GS-Hider often appears blurry in these areas. Meanwhile, 3DGS+StegaNeRF is more inclined to remember the embedded copyright image because it is decoded from the rendered RGB view, which will cause severe aliasing and interference of the rendered view and copyright image.

## 5 CONCLUSION

In this paper, we propose SecureGS, a novel and efficient 3DGS steganography framework. SecureGS successfully addresses the challenges of security and fidelity in previous 3DGS steganography approaches by incorporating anchor point-based neural decoding, a hybrid Gaussian encryption mechanism, and a region-aware density optimization. Our approach allows for secure embedding and retrieval of hidden 3D content, copyright images, and bits, ensuring high fidelity in rendering both the original and hidden message. Extensive experiments confirm that our SecureGS outperforms existing methods in rendering speed, fidelity, and security, showcasing its potential for real-time applications. Furthermore, our work lays a promising foundation for advancements in copyright protection and encrypted transmission of 3D assets, offering a new avenue for safeguarding 3D content in various digital media landscapes.

## REFERENCES

- 540  
541  
542 Shumeet Baluja. Hiding images within images. *IEEE transactions on pattern analysis and machine*  
543 *intelligence*, 42(7):1685–1697, 2019.
- 544 Jonathan T Barron, Ben Mildenhall, Matthew Tancik, Peter Hedman, Ricardo Martin-Brualla, and  
545 Pratul P Srinivasan. Mip-nerf: A multiscale representation for anti-aliasing neural radiance fields.  
546 In *Proceedings of the IEEE/CVF International Conference on Computer Vision*, pp. 5855–5864,  
547 2021.
- 548 Abbas Cheddad, Joan Condell, Kevin Curran, and Paul Mc Kevitt. Digital image steganography:  
549 Survey and analysis of current methods. *Signal processing*, 90(3):727–752, 2010.
- 550  
551 Guangyu Chen, Yu Wu, Shujie Liu, Tao Liu, Xiaoyong Du, and Furu Wei. Wavmark: Watermarking  
552 for audio generation. *arXiv preprint arXiv:2308.12770*, 2023.
- 553  
554 Martin Ester, Hans-Peter Kriegel, Jörg Sander, Xiaowei Xu, et al. A density-based algorithm for  
555 discovering clusters in large spatial databases with noise. In *kdd*, volume 96, pp. 226–231, 1996.
- 556 Pierre Fernandez, Guillaume Couairon, Hervé Jégou, Matthijs Douze, and Teddy Furon. The stable  
557 signature: Rooting watermarks in latent diffusion models. In *Proceedings of the IEEE/CVF*  
558 *International Conference on Computer Vision*, pp. 22466–22477, 2023.
- 559 Youngdong Jang, Dong In Lee, MinHyuk Jang, Jong Wook Kim, Feng Yang, and Sangpil Kim.  
560 Waterf: Robust watermarks in radiance fields for protection of copyrights. In *Proceedings of the*  
561 *IEEE conference on computer vision and pattern recognition*, 2024a.
- 562  
563 Youngdong Jang, Hyunje Park, Feng Yang, Heeju Ko, Euijin Choo, and Sangpil Kim. 3d-gsw:  
564 3d gaussian splatting watermark for protecting copyrights in radiance fields. *arXiv preprint*  
565 *arXiv:2409.13222*, 2024b.
- 566 Nikhil Keetha, Jay Karhade, Krishna Murthy Jatavallabhula, Gengshan Yang, Sebastian Scherer,  
567 Deva Ramanan, and Jonathon Luiten. Splatam: Splat, track & map 3d gaussians for dense rgb-d  
568 slam. *arXiv preprint arXiv:2312.02126*, 2023.
- 569  
570 Bernhard Kerbl, Georgios Kopanas, Thomas Leimkühler, and George Drettakis. 3d gaussian splatting  
571 for real-time radiance field rendering. *ACM Transactions on Graphics*, 42(4):1–14, 2023.
- 572 Chenxin Li, Brandon Y Feng, Zhiwen Fan, Panwang Pan, and Zhangyang Wang. Steganerf: Em-  
573 bedding invisible information within neural radiance fields. In *Proceedings of the IEEE/CVF*  
574 *International Conference on Computer Vision*, pp. 441–453, 2023a.
- 575  
576 Chenxin Li, Hengyu Liu, Zhiwen Fan, Wuyang Li, Yifan Liu, Panwang Pan, and Yixuan Yuan.  
577 Gaussianstego: A generalizable stenography pipeline for generative 3d gaussians splatting. *arXiv*  
578 *preprint arXiv:2407.01301*, 2024.
- 579 Zhan Li, Zhang Chen, Zhong Li, and Yi Xu. Spacetime gaussian feature splatting for real-time  
580 dynamic view synthesis. *arXiv preprint arXiv:2312.16812*, 2023b.
- 581  
582 Chang Liu, Jie Zhang, Han Fang, Zehua Ma, Weiming Zhang, and Nenghai Yu. Dear: A deep-  
583 learning-based audio re-recording resilient watermarking. In *Proceedings of the AAAI Conference*  
584 *on Artificial Intelligence*, volume 37, pp. 13201–13209, 2023a.
- 585  
586 Chang Liu, Jie Zhang, Tianwei Zhang, Xi Yang, Weiming Zhang, and Nenghai Yu. Detecting voice  
587 cloning attacks via timbre watermarking. *arXiv preprint arXiv:2312.03410*, 2023b.
- 588  
589 Tao Lu, Mulin Yu, Linning Xu, Yuanbo Xiangli, Limin Wang, Dahua Lin, and Bo Dai. Scaffold-gs:  
590 Structured 3d gaussians for view-adaptive rendering. In *Proceedings of the IEEE/CVF Conference*  
591 *on Computer Vision and Pattern Recognition*, 2023.
- 592  
593 Jonathon Luiten, Georgios Kopanas, Bastian Leibe, and Deva Ramanan. Dynamic 3d gaussians:  
Tracking by persistent dynamic view synthesis. *arXiv preprint arXiv:2308.09713*, 2023.
- Xiyang Luo, Yinxiao Li, Huiwen Chang, Ce Liu, Peyman Milanfar, and Feng Yang. Dvmark: a deep  
multiscale framework for video watermarking. *IEEE Transactions on Image Processing*, 2023a.

- 594 Ziyuan Luo, Qing Guo, Ka Chun Cheung, Simon See, and Renjie Wan. Copyrnerf: Protecting the  
595 copyright of neural radiance fields. In *Proceedings of the IEEE/CVF International Conference on*  
596 *Computer Vision*, pp. 22401–22411, 2023b.
- 597 Hidenobu Matsuki, Riku Murai, Paul HJ Kelly, and Andrew J Davison. Gaussian splatting slam.  
598 *arXiv preprint arXiv:2312.06741*, 2023.
- 600 B Mildenhall, PP Srinivasan, M Tancik, JT Barron, R Ramamoorthi, and R Ng. Nerf: Representing  
601 scenes as neural radiance fields for view synthesis. In *European conference on computer vision*,  
602 2020.
- 603 Ryutarou Ohbuchi, Akio Mukaiyama, and Shigeo Takahashi. A frequency-domain approach to  
604 watermarking 3d shapes. In *Computer graphics forum*, volume 21, pp. 373–382. Wiley Online  
605 Library, 2002.
- 607 Xuran Pan, Zhuofan Xia, Shiji Song, Li Erran Li, and Gao Huang. 3d object detection with point-  
608 former. In *Proceedings of the IEEE/CVF conference on computer vision and pattern recognition*,  
609 pp. 7463–7472, 2021.
- 610 Emil Praun, Hugues Hoppe, and Adam Finkelstein. Robust mesh watermarking. In *Proceedings of*  
611 *the 26th annual conference on Computer graphics and interactive techniques*, pp. 49–56, 1999.
- 612 Niels Provos and Peter Honeyman. Hide and seek: An introduction to steganography. *IEEE security*  
613 *& privacy*, 1(3):32–44, 2003.
- 614 Robin San Roman, Pierre Fernandez, Alexandre Défossez, Teddy Furon, Tuan Tran, and Hady Elsahar.  
615 Proactive detection of voice cloning with localized watermarking. *arXiv preprint arXiv:2401.17264*,  
616 2024.
- 617 Qi Song, Ziyuan Luo, Ka Chun Cheung, Simon See, and Renjie Wan. Protecting nerfs’ copyright via  
618 plug-and-play watermarking base model. *arXiv preprint arXiv:2407.07735*, 2024.
- 619 Jiaxiang Tang, Jiawei Ren, Hang Zhou, Ziwei Liu, and Gang Zeng. Dreamgaussian: Generative  
620 gaussian splatting for efficient 3d content creation. *arXiv preprint arXiv:2309.16653*, 2023.
- 621 Yuxin Wen, John Kirchenbauer, Jonas Geiping, and Tom Goldstein. Tree-rings watermarks: Invisible  
622 fingerprints for diffusion images. *Advances in Neural Information Processing Systems*, 36, 2024.
- 623 Guanjun Wu, Taoran Yi, Jiemin Fang, Lingxi Xie, Xiaopeng Zhang, Wei Wei, Wenyu Liu, Qi Tian,  
624 and Xinggang Wang. 4d gaussian splatting for real-time dynamic scene rendering. *arXiv preprint*  
625 *arXiv:2310.08528*, 2023.
- 626 Zhirong Wu, Shuran Song, Aditya Khosla, Fisher Yu, Linguang Zhang, Xiaoou Tang, and Jianxiong  
627 Xiao. 3d shapenets: A deep representation for volumetric shapes. In *Proceedings of the IEEE*  
628 *conference on computer vision and pattern recognition*, pp. 1912–1920, 2015.
- 629 Shuzhou Yang, Yu Wang, Haijie Li, Jiarui Meng, Xiandong Meng, and Jian Zhang. Fourier123: One  
630 image to high-quality 3d object generation with hybrid fourier score distillation. *arXiv preprint*  
631 *arXiv:2405.20669*, 2024a.
- 632 Ziyi Yang, Xinyu Gao, Wen Zhou, Shaohui Jiao, Yuqing Zhang, and Xiaogang Jin. Deformable 3d  
633 gaussians for high-fidelity monocular dynamic scene reconstruction. *Proceedings of the IEEE/CVF*  
634 *Conference on Computer Vision and Pattern Recognition (CVPR)*, 2024b.
- 635 Taoran Yi, Jiemin Fang, Junjie Wang, Guanjun Wu, Lingxi Xie, Xiaopeng Zhang, Wenyu Liu, Qi Tian,  
636 and Xinggang Wang. Gaussiandreamer: Fast generation from text to 3d gaussians by bridging 2d  
637 and 3d diffusion models. In *Proceedings of the IEEE/CVF Conference on Computer Vision and*  
638 *Pattern Recognition (CVPR)*, 2024.
- 639 Innfarn Yoo, Huiwen Chang, Xiyang Luo, Ondrej Stava, Ce Liu, Peyman Milanfar, and Feng Yang.  
640 Deep 3d-to-2d watermarking: Embedding messages in 3d meshes and extracting them from  
641 2d renderings. In *Proceedings of the IEEE/CVF Conference on Computer Vision and Pattern*  
642 *Recognition (CVPR)*, pp. 10031–10040, June 2022.

648 Jiwen Yu, Xuanyu Zhang, Youmin Xu, and Jian Zhang. Cross: Diffusion model makes controllable,  
649 robust and secure image steganography. *Advances in Neural Information Processing Systems*, 36,  
650 2023a.

651 Zehao Yu, Anpei Chen, Binbin Huang, Torsten Sattler, and Andreas Geiger. Mip-splatting: Alias-free  
652 3d gaussian splatting. In *Proceedings of the IEEE/CVF Conference on Computer Vision and*  
653 *Pattern Recognition*, 2023b.

654 Xuanyu Zhang, Runyi Li, Jiwen Yu, Youmin Xu, Weiqi Li, and Jian Zhang. Editguard: Versatile  
655 image watermarking for tamper localization and copyright protection. In *Proceedings of the IEEE*  
656 *conference on computer vision and pattern recognition*, 2024a.

657 Xuanyu Zhang, Jiarui Meng, Runyi Li, Zhipei Xu, Yongbing Zhang, and Jian Zhang. Gs-hider:  
658 Hiding messages into 3d gaussian splatting. *Advances in Neural Information Processing Systems*,  
659 2024b.

660 Xuanyu Zhang, Youmin Xu, Runyi Li, Jiwen Yu, Weiqi Li, Zhipei Xu, and Jian Zhang. V2a-mark:  
661 Versatile deep visual-audio watermarking for manipulation localization and copyright protection.  
662 In *Proceedings of the ACM International Conference on Multimedia (ACM MM)*, 2024c.

663 Jiren Zhu, Russell Kaplan, Justin Johnson, and Li Fei-Fei. Hidden: Hiding data with deep networks.  
664 In *Proceedings of the European conference on computer vision (ECCV)*, pp. 657–672, 2018.

665 Matthias Zwicker, Hanspeter Pfister, Jeroen Van Baar, and Markus Gross. Ewa volume splatting. In  
666 *IEEE Conference on Visualization (VIS)*, 2001.

667  
668  
669  
670  
671  
672  
673  
674  
675  
676  
677  
678  
679  
680  
681  
682  
683  
684  
685  
686  
687  
688  
689  
690  
691  
692  
693  
694  
695  
696  
697  
698  
699  
700  
701

## A APPENDIX

### A.1 MORE IMPLEMENTATION DETAILS

**Dataset Construction:** To make the training view set of the hidden object and the original scene correspond to each other, we use the Supersplat to align the position of the original scene and hidden object and render the training set of the hidden object according to the viewpoints in the training set of the original scene. The correspondence between the hidden object and original scenes is listed in Tab. 6.

Table 6: Correspondence between hidden objects and original scenes.

Original Scene	Bicycle	Flowers	Garden	Stump	Treehill	Room	Counter	Kitchen	Bonsai
Hidden Object	hotdog	lego	ficus	drums	ficus	chair	lego	ship	mic

#### Implementation Details and Network Structure:

Feature bank: We follow the design of the feature bank introduced in Scaffold-GS (Lu et al., 2023) to extend  $\mathbf{f}_v$  to be multi-resolution and view-dependent feature  $\hat{\mathbf{f}}_v$ . Specifically, for each anchor  $v$ , we generate a feature bank  $\{\mathbf{f}_v, \mathbf{f}_{v_{\downarrow 1}}, \mathbf{f}_{v_{\downarrow 2}}\}$ , which is then fused using view-dependent weights to obtain a combined anchor feature  $\hat{\mathbf{f}}_v$ . Given the camera located at  $\mathbf{x}_c$  and an anchor at  $\mathbf{x}_v$ , we compute their relative distance and viewing direction as follows:

$$\delta_{vc} = \|\mathbf{x}_v - \mathbf{x}_c\|_2, \quad \vec{d}_{vc} = \frac{\mathbf{x}_v - \mathbf{x}_c}{\|\mathbf{x}_v - \mathbf{x}_c\|_2}, \quad (9)$$

The feature bank is then blended through a weighted sum, with the weights predicted by a small MLP  $\mathcal{F}_w$ . The integrated anchor feature  $\hat{\mathbf{f}}_v$  is then calculated as:

$$\{w, w_1, w_2\} = \text{Softmax}(\mathcal{F}_w(\delta_{vc}, \vec{d}_{vc})), \quad (10)$$

$$\hat{\mathbf{f}}_v = w \cdot \mathbf{f}_v + w_1 \cdot \mathbf{f}_{v_{\downarrow 1}} + w_2 \cdot \mathbf{f}_{v_{\downarrow 2}}. \quad (11)$$

The structure of MLPs: The structure of our MLPs follows a “Linear  $\rightarrow$  RELU  $\rightarrow$  Linear” style with the hidden dimension of 32. The structure of  $\{\mathcal{F}_\alpha^\dagger, \mathcal{F}_s^\dagger, \mathcal{F}_q^\dagger, \mathcal{F}_c^\dagger\}$  is identical to  $\{\mathcal{F}_\alpha, \mathcal{F}_s, \mathcal{F}_q, \mathcal{F}_c\}$  in Scaffold-GS. Note that for the offset predictor  $\mathcal{F}_o^\dagger$ , the last linear layer is to transform intermediate tensors from  $\mathbb{R}^{N \times 32}$  to  $\mathbb{R}^{N \times (3k)}$ , where  $N$  and  $k$  respectively denote the number of anchor points and hidden Gaussian points generated by each voxel.

**The algorithm of our RDO Strategy:** To more clearly demonstrate our region-aware density optimization (RDO) algorithm, we have provided the pseudocode in Alg. 1.

### A.2 RELATIONSHIPS AND DIFFERENCES WITH EXISTING 3D STEGANOGRAPHY METHODS

**Comparison with GS-Hider:** Our SecureGS and GS-Hider (Zhang et al., 2024b) follow similar task setups, assuming that the point cloud file needs to be publicly available while hiding information. At a high level, SecureGS and GS-Hider adopt a “coupling-decoupling” process. **The main differences** between them lie in the implementation architecture: First, GS-Hider is built on the original 3DGS and embeds information through coupled feature attributes, using a CNN-based neural network to decode the feature maps. The decoding mechanism from feature maps is the root cause of its deficiencies in security, fidelity, and rendering speed. In contrast, our SecureGS is built on the efficient Scaffold-GS, which naturally generates Gaussian points from anchor points specifically for rendering hidden information. Additionally, we use several MLPs to efficiently and in parallel decode the anchor point cloud in batches. Thanks to our efficient mechanism of decoding from anchor points and the proposed region-aware density optimization, we outperform GS-Hider in all aspects. Our method improves fidelity by over 1dB, renders scenes twice as fast as GS-Hider, and requires less storage space while ensuring both the format and geometric structure security of the point cloud files. Additionally, GS-Hider does not support bit embedding and decoding, a limitation that we have addressed in our approach.

**Comparison with HiDDeN-based Methods:** Most previous SOTA 3D watermarking methods (Luo et al., 2023b; Jang et al., 2024a;b; Song et al., 2024) typically use a watermark decoder pre-trained

Table 7: Comparison of 3D scene hiding between GS-Hider and SecureGS.

Method	PSNR <sub>o</sub> (dB)	SSIM <sub>o</sub>	LPIPS <sub>o</sub>	PSNR <sub>s</sub> (dB)	SSIM <sub>s</sub>	LPIPS <sub>s</sub>
GS-Hider	25.82	0.783	0.246	25.18	0.780	0.306
SecureGS	27.20	0.796	0.235	29.75	0.858	0.211

on the image domain (e.g., HiDDeN (Zhu et al., 2018)). This watermark decoder is tasked with extracting bits from rendered views by NeRF or 3DGS, offering excellent generalization in message extraction. In contrast, our SecureGS aims to decode bit information directly from the point cloud, which aligns better with the explicit representation features of 3DGS and is more direct and efficient. Currently, there are no deep networks capable of embedding and decoding bits from point clouds, which makes it infeasible for us to adopt HiDDeN-based methods for generalized message extraction. However, our message extraction MLP is lightweight enough that it does not increase training time or cost. We plan to explore the development of a generalized method for extracting bits directly from point clouds in future work.

### A.3 LIMITATIONS AND FUTURE WORKS

**Limitations:** First, to enhance the geometric security of our method, we have to promote anchor point splitting to some extent through our RDO strategy, which results in slightly larger storage space compared to the original Scaffold-GS when hiding 3D objects. Second, to better ensure the security of our steganography framework, the hidden object is required to partially overlap with the point cloud of the original scene to some extent. Hiding a 3D object without leaving traces in areas where the original point cloud is sparse is extremely difficult and remains an area for further exploration.

**Future works:** Our future work will focus primarily on improving the robustness of 3DGS steganography, ensuring that the hidden object’s integrity and fidelity are preserved even under more severe damage and aggressive pruning strategies. Additionally, we will explore leveraging 3D backbone networks, such as PointFormer (Pan et al., 2021), to directly decode the hidden point cloud from the original Gaussian points, further enhancing the security of 3D steganography through structured and network-based approaches.

### A.4 RESULTS ON HIDING 3D SCENE INTO 3D SCENE

Following the setup of GS-Hider, we compare our SecureGS with GS-Hider on hiding 3D scenes into 3D scenes. Here, we do not use the bounding box in the RDO strategy, as it is not meaningful for high-capacity scene hiding. The results are reported on Tab. 7. It can be observed that the rendering fidelity of the original scene and the hidden scene in our method is 1.38 dB and 4.57 dB higher than that of GS-Hider, respectively, demonstrating a significant advantage.

### A.5 MORE ROBUSTNESS ANALYSIS

To further validate the robustness of our method, we apply several 3D degradations to the anchor point cloud, including Gaussian noise of varying intensities and point cloud denoising. The metrics are reported on Tab. 8. The Gaussian noise intensities are set to 0.05, 0.1, and 0.15, and the denoising method is Statistical Outlier Removal. It can be observed that our method demonstrates strong resistance to Gaussian noise. Moreover, when dealing with point cloud denoising, although the original scene’s rendering quality decreases, the hidden object’s rendering quality remains almost unchanged. Fig. 10 further illustrates the robustness of our method under different degradations.

### A.6 MORE ABLATION STUDIES

To further clarify the independent contributions of our region-aware density optimization (RDO), we further conduct ablation studies on RDO and realize two variants, namely globally reducing the gradient threshold and using the same gradient to grow anchor points representing both the original and hidden scenes. The results are reported on Tab. 9. We find that globally lowering the gradient threshold increases the memory size by 114.76 MB, significantly reducing rendering speed

Table 8: PSNR (dB) and SSIM under different degradation conditions.

Condition	PSNR <sub>o</sub>	SSIM <sub>o</sub>	PSNR <sub>s</sub>	SSIM <sub>s</sub>
Clean	27.93	0.822	38.21	0.986
Gaussian noise ( $\sigma=0.05$ )	27.87	0.820	37.52	0.984
Gaussian noise ( $\sigma=0.1$ )	27.74	0.817	37.04	0.983
Gaussian noise ( $\sigma=0.15$ )	27.55	0.857	36.18	0.981
Point cloud denoising	24.02	0.794	38.20	0.986

Table 9: Ablation study on different key steps in the region-aware density optimization.

Method	Memory Size (MB)	PSNR <sub>o</sub> (dB)	SSIM <sub>o</sub>	PSNR <sub>s</sub> (dB)	SSIM <sub>s</sub>
Globally reducing the gradient threshold	405.27	28.11	0.831	38.36	0.987
Using the same gradient for anchor growing	252.49	27.73	0.815	37.95	0.977
SecureGS (Ours)	290.54	27.93	0.822	38.21	0.986

while only resulting in a 0.18 dB gain in PSNR. Additionally, if a shared gradient is used instead of our asynchronous gradient accumulation, the rendering of the original scene and the hidden object interferes with each other, leading to a reduction in rendering quality for both and failing to ensure security. Thus, our region-aware density optimization achieves a well-balanced trade-off between rendering quality, security, and rendering efficiency.

Furthermore, we also present the visualized results of point cloud produced by our baseline “Ours w/o RDO and HDGER” in Fig. 9. “Ours w/o RDO and HDGER” denotes directly adding the offset  $O_{v \otimes j}^{hid}$  to the point cloud file and using a series of encrypted MLPs to predict the attributes of the hidden Gaussian points. Meanwhile, the anchor growing and reduction strategy is the same as Scaffold-GS. Quantitative metrics are reported in Tab. 4. Although this method achieves acceptable fidelity for both the hidden object and the original scene, its point cloud completely exposes the information of the hidden object, failing to meet the security requirements of 3DGS steganography. This indicates that simply combining the framework design of GS-Hider with the rendering method of Scaffold-GS cannot achieve steganography with strong security.



Figure 9: Visualized results of the point cloud produced by “Ours w/o RDO and HDGER”.

### A.7 MORE VISUALIZATION RESULTS

We present more visualization results of our rendering results under different degradations in Fig. 11, the rendering results of bit hiding in Fig. 12, the rendering results of single image hiding in Fig. 13, and the results of 3D object hiding in Fig. 14.



864  
865  
866  
867  
868  
869  
870  
871  
872  
873  
874  
875  
876  
877  
878  
879  
880  
881  
882  
883  
884  
885  
886  
887  
888  
889  
890  
891  
892  
893  
894  
895  
896  
897  
898  
899  
900  
901  
902  
903  
904  
905  
906  
907  
908  
909  
910  
911  
912  
913  
914  
915  
916  
917

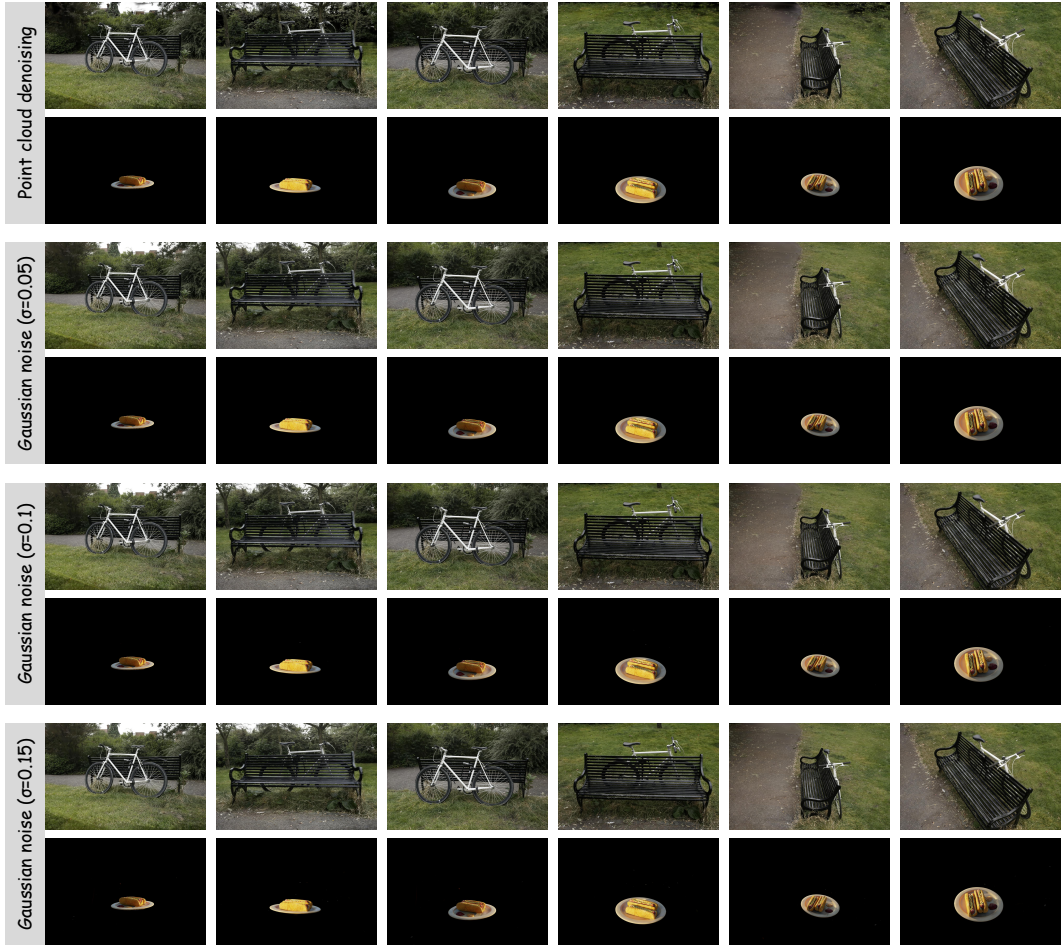


Figure 10: Rendered results of the original scene and hidden object produced by our SecureGS under Gaussian noise and point cloud denoising.

**Algorithm 1** Overall Pipeline of Our Proposed Region-Aware Density Optimization

```

918
919
920  $i \leftarrow 0$  ▷ Iteration Count
921  $\Gamma_{ori} \leftarrow$  SfM points ▷ Initialization of the anchor point set produced based on  $\nabla_{ori}$ 
922  $\Gamma_{hid} = \{\}$  ▷ Initialization of the anchor point set produced based on  $\nabla_{hid}$ 
923 while not converged do
924    $\ell_{total} = \ell_{ori} + \lambda \ell_{hid}$  ▷ Computed via Eq. 8
925    $\nabla_{ori} \leftarrow$  AccumulateGradient( $\nabla \ell_{total}$ ),
926   if  $i \% \text{step} == 0$  then:
927      $\nabla_{hid} \leftarrow$  AccumulateGradient( $\nabla \ell_{total}$ ), ▷ Accumulate gradients in different intervals
928   end if
929   if IsRefinementIteration( $i$ ) then
930     if IsBoundingBoxIteration( $i$ ) then
931        $\mathbb{S}_{bbx} \leftarrow$  PointCloudCluster( $\Gamma_{hid}$ ) ▷ Using the clustering method to get a bounding box
932     end if
933     for all anchor points  $v(\mathbf{x}_v, \mathbf{f}_v, l_v, O_v^{ori})$  in  $\Gamma_{ori} \cup \Gamma_{hid}$  do
934       if  $v \in \mathbb{S}_{bbx}$  then
935          $\tau_{ada} = \tau_{fix} / r_{down}$  ▷ Lower the threshold if the anchor in the bounding box
936       end if
937       if  $\nabla_{ori} > \tau_{ada}$  then
938          $\Gamma_{ori} \leftarrow$  AnchorGrowing( $\Gamma_{ori}$ )
939          $\Gamma_{ori}, \Gamma_{hid} \leftarrow$  AnchorPruning( $\Gamma_{ori}, \Gamma_{hid}$ )
940       end if
941       if  $\nabla_{hid} > \tau_{fix}$  then
942          $\Gamma_{hid} \leftarrow$  AnchorGrowing( $\Gamma_{hid}$ )
943       end if
944     end for
945   end if
946    $i \leftarrow i + 1$ 
947 end while

```

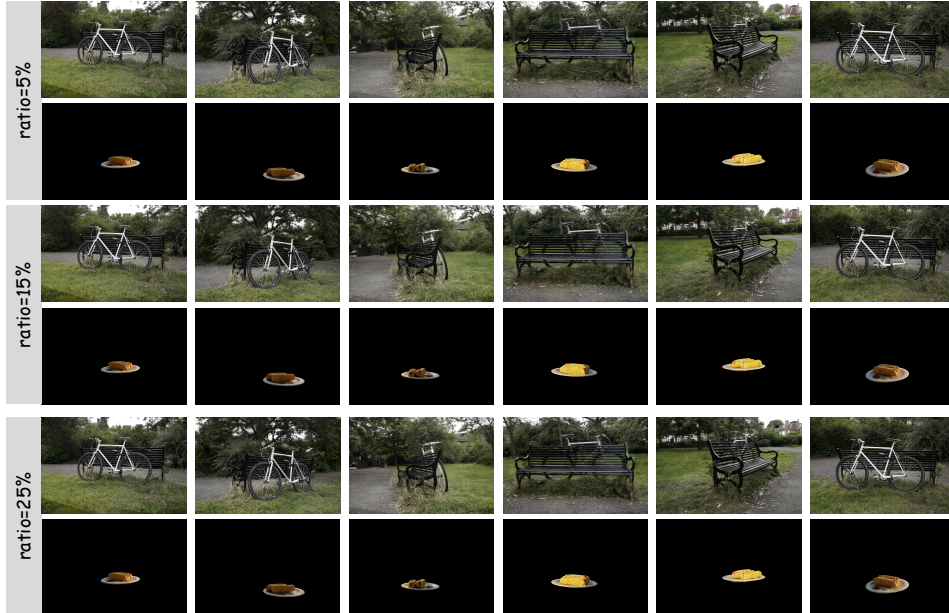


Figure 11: Rendered results of the original scene and hidden object produced by our SecureGS under different degradations.

972

973

974

975

976

977

978

979

980

981

982

983

984

985

986

987

988

989

990

991

992

993

994

995

996

997

998

999

1000

1001

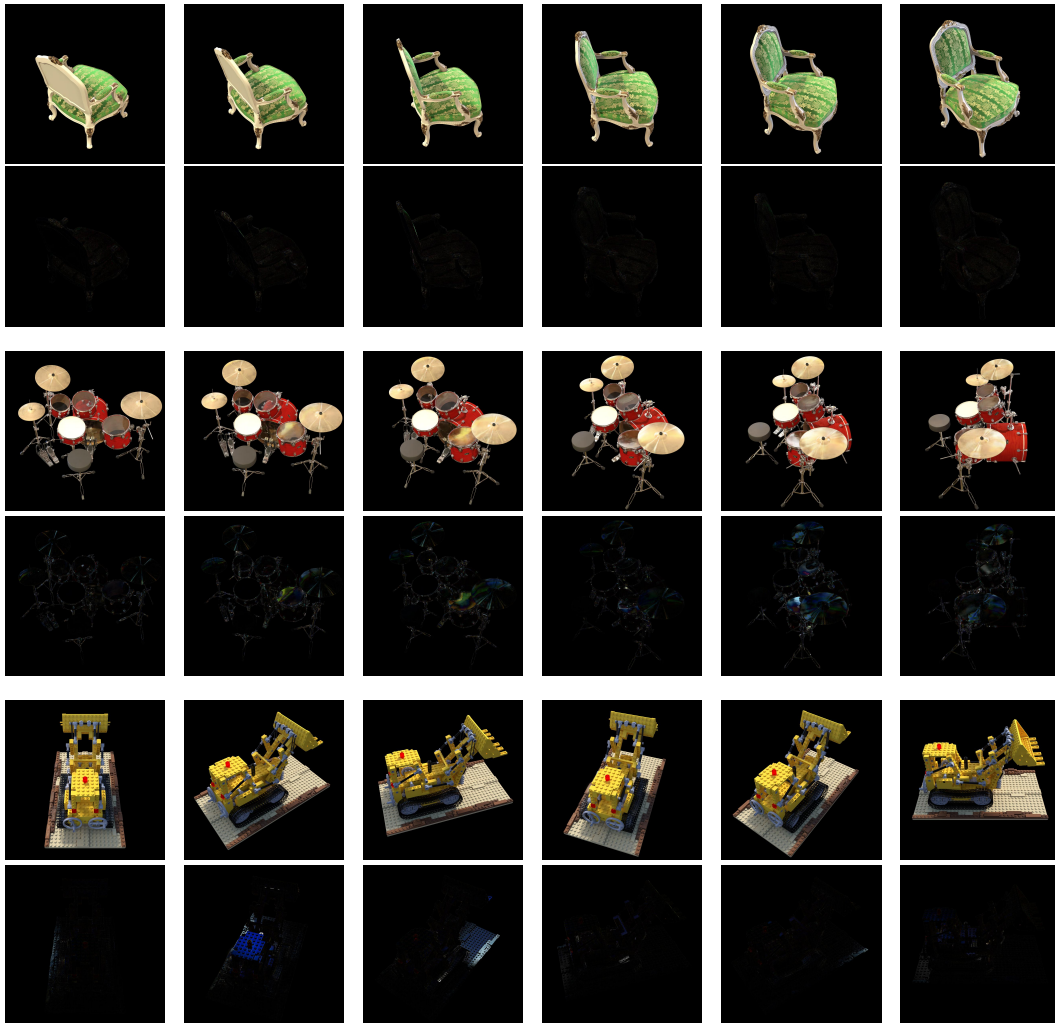
1002

1003

1004

1005

1006



1007

1008

1009

1010

1011

1012

Figure 12: Rendered object and error maps produced by the proposed SecureGS on the blender dataset. After embedding the bit message, the rendering quality of our original scene will hardly be affected.

1013

1014

1015

1016

1017

1018

1019

1020

1021

1022

1023

1024

1025



Figure 13: Rendered view and recovered different copyright images produced by our SecureGS.

1026  
1027  
1028  
1029  
1030  
1031  
1032  
1033  
1034  
1035  
1036  
1037  
1038  
1039  
1040  
1041  
1042  
1043  
1044  
1045  
1046  
1047  
1048  
1049  
1050  
1051  
1052  
1053  
1054  
1055  
1056  
1057  
1058  
1059  
1060  
1061  
1062  
1063  
1064  
1065  
1066  
1067  
1068  
1069  
1070  
1071  
1072  
1073  
1074  
1075  
1076  
1077  
1078  
1079

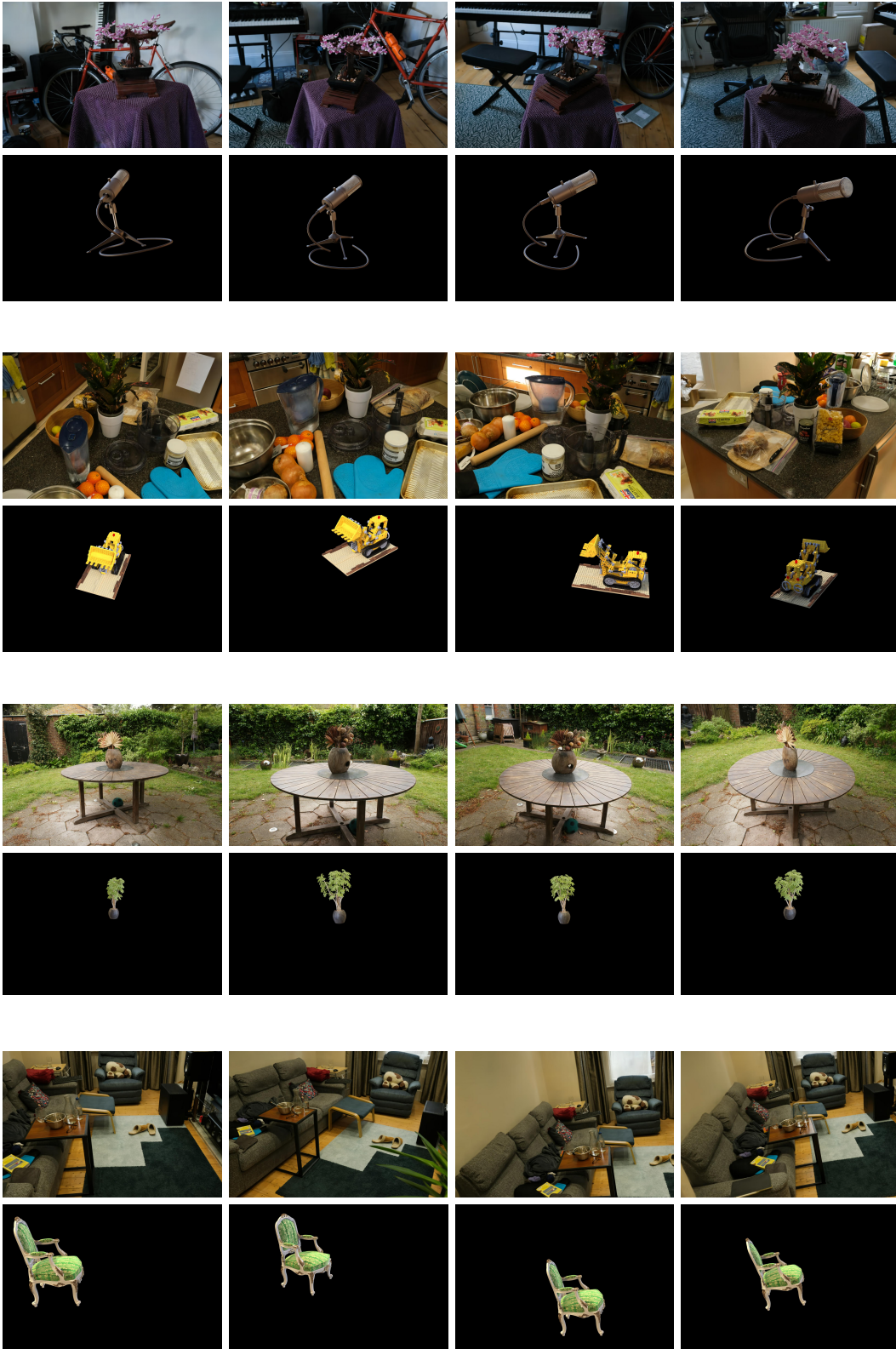


Figure 14: Rendered original scene and the hidden object produced by our SecureGS. The first row of each group is the original scene and the second row is the hidden object.